Exchange spring switching in Er-doped $DyFe_2/YFe_2$ magnetic thin films

G. B. G. Stenning,[1,2] G. J. Bowden,[1] P. A. J. de Groot,[1] G. van der Laan,[3,*] A. I. Figueroa,[3] P. Bencok,[4] P. Steadman,[4] and T. Hesjedal[4,5,†]

[1]*School of Physics and Astronomy, University of Southampton, SO17 1BJ, United Kingdom*
[2]*ISIS Neutron and Muon Source, Rutherford Appleton Laboratory, Didcot OX11 0QX, United Kingdom*
[3]*Magnetic Spectroscopy group, Diamond Light Source, Didcot OX11 0DE, United Kingdom*
[4]*Diamond Light Source, Science Division, Didcot OX11 0DE, United Kingdom*
[5]*Department of Physics, Clarendon Laboratory, University of Oxford, Oxford OX1 3PU, United Kingdom*

(Received 21 April 2015; revised manuscript received 17 June 2015; published 8 September 2015)

Reversible magnetic exchange springs can be formed in multilayer films, grown by molecular beam epitaxy. Here we demonstrate that small amounts of anisotropic $ErFe_2$, placed in the middle of the YFe_2 magnetic exchange springs, can bring about substantial changes. Results are presented for an Er-doped (110)-oriented multilayer film, at 100 K in fields of up to ± 14 T. Using both Er and Dy-specific soft x-ray magnetic circular dichroism and micromagnetic modeling, it is demonstrated that Er doping gives rise to (*i*) noncollinear exchange spring states in zero field, (*ii*) magnetic exchange spring collapse, (*iii*) a marked increase in the number of different exchange spring states available to the system, and (*iv*) strikingly different Er and Dy magnetization loops. Full and partial loops are presented for both the in-plane hard and easy axes. The magnetization loops for Dy sublattice show that at least ten different exchange spring states are accessed during magnetic reversal. Magnetic switching scenarios, involving mixtures of Néel-like and Bloch-like domain walls, are presented and discussed.

DOI: 10.1103/PhysRevB.92.104404 PACS number(s): 68.65.Ac, 75.60.Ch, 75.30.Gw, 78.70.Dm

I. INTRODUCTION

In the field of magnetic switching the formation of magnetic domain walls, their pinning and movement, play a fundamental role. In general, they are usually described in terms Néel- and Bloch-like domain walls [1]. In many applications, domain walls which move freely in small magnetic fields are very desirable. For example, low-loss alloys such as permalloy have found numerous applications in transformers and magnetic shielding [2]. However, in the case of permanent magnets, the opposite is true. Here efforts are made to "pin" domain walls, in order to increase the maximum energy product, $(\mathbf{B}\cdot\mathbf{H})_{\max}$. For example, in the 1990s, great efforts were made to develop so-called exchange spring magnets [3–6]. Here the high magnetic moment of soft iron is combined with high coercivity magnets such as $Nd_2Fe_{14}B$, to give the best of both worlds. However, despite intensive efforts, both in Europe and the USA, such dreams have only been partially realized [7]. In short, incipient exchange springs set up in the soft Fe layers exert strong torques on the hard layers, leading to a reduction in the coercive field. However, one possible way of overcoming this problem is to place pinning centers directly into the middle of the soft exchange springs. Such pinning centers render the springs irreversible and dramatically affect their properties in applied magnetic fields.

In this paper, domain wall pinning is examined in a molecular beam epitaxy (MBE) grown [$DyFe_2$ (60 Å)/YFe_2 (240 Å)]$_{15}$ multilayer film, doped with an 8-Å-thick anisotropic $ErFe_2$ layer. Using applied magnetic fields, reversible magnetic exchange springs (model domain walls) are easily set up in the magnetically soft YFe_2 layers [8,9]. However, when small amounts of anisotropic $ErFe_2$ are placed in the center of the YFe_2 magnetic exchange springs, the domain walls become pinned and are no longer reversible. In the Er doped multilayer system, it will be shown that the domain walls are characterized by both in-plane (Néel) walls and out-of-plane (Bloch) walls. In practice, the identification of such spin states is nontrivial. Here, the use of element-specific x-ray magnetic circular dichroism (XMCD) is decisive [10]. It allows the reversal processes of both the hard pinning Dy layers and the Er domain-wall pinning layers to be studied independently. This represents a huge advantage over conventional bulk magnetization measurements, which can only yield the net magnetic moment of all the elements combined [11].

The first XMCD studies on $DyFe_2/YFe_2$ exchange spring systems were undertaken by Dumesnil *et al.* [12,13]. In particular, they performed Dy- and Y-XMCD studies on a [$DyFe_2$ (50 Å)/YFe_2 (200 Å)] multilayer, in an attempt to define the spin configurations around the magnetization loop [13]. Based on their element-selective loops, they proposed various field-dependent spin configurations for two differing regimes: (*i*) where the coercivity is negative (100 K) and (*ii*) where the coercivity is positive (200 K) (Fig. 1 of Ref. [13]). Briefly, at 100 K in large fields applied along an easy in-plane Dy [001] axis, the magnetization loop is characterized by Dy moments aligned along the [001] axis accompanied by a strong in-plane magnetic exchange spring in the soft YFe_2 layers. As the field is reduced the spring unwinds leading to a simple net antiferromagnetic (AF) state [14]. Finally, in a negative field of $\sim$6 T there is a switch to the reversed magnetic state.

However, it is now known that the actual reversal mechanism is much more complex. Recent XMCD experiments [15,16] have shown that reversal, in an almost identical [$DyFe_2$ (60 Å)/YFe_2 (240 Å)] multilayer at 100 K, involves the presence of more than just in-plane magnetic exchange springs. In particular, magnetic reversal occurs via a two-step process involving an intermediate *transverse* exchange spring state, characterized by an out-of-plane Dy [010] easy axis (see also Ref. [17]). The situation at 200 K is even more complex,

*Gerrit.vanderLaan@diamond.ac.uk
†Corresponding author: Thorsten.Hesjedal@physics.ox.ac.uk

and will not be discussed here. For the present, we simply note that the suggested spin configurations at 100 K [13] only involve in-plane Néel walls or in-plane AF states. However, given the existence of out-of-plane Bloch-like walls [15,16], the interpretation of Ref. [13] clearly warrants reexamination.

More recently, bulk magnetization and XMCD studies on a nominally [$DyFe_2$ (60 Å)/YFe_2 (240 Å)] multilayer have been taken to a new level [11,18]. By placing a thin $DyFe_2$ layer in the middle of the magnetically soft YFe_2 layers, new opportunities arise. For example, very dilute Dy doping could be used as a probe to see what happens at the center of an exchange spring. Alternatively, heavier Dy doping can be used to profoundly modify the properties of the magnetic exchange springs. In particular, it has been demonstrated that doping with an 8-Å-thick $DyFe_2$ layer renders the exchange springs irreversible, increasing the number of steps involved in the magnetic reversal mechanism from two to four, and sharply increasing the number of spin configurations available to the multilayer. In practice, a good working knowledge of the available domain walls is essential, if the aspirations of Refs. [3–6] are ever to be realized. Of course, in the case of the RFe_2/YFe_2 multilayers (R = rare earth) it is highly unlikely that they will ever be used as hard magnetic materials, because of their low net-magnetic moments. Nevertheless, it is well known that they do form an ideal test bed for domain wall studies [19].

The outline of the remainder of this paper is as follows. In Sec. II we give an overview of the possible exchange spring states, and in Sec. III we discuss the experimental details of the sample growth and the XMCD measurements. Section IV presents the experimental results and Sec. V details about the micromagnetic model. In Sec. VI a discussion of the magnetic switching for a field applied an easy axis is presented, and the corresponding discussion for a hard axis direction is given in Appendix C. Section VII introduces a simple explanation of the exchange spring collapse, and Sec. VIII discusses a comparison between Er- and Dy-doped samples, before we summarize the results in Sec. IX.

II. NUMBER OF EXCHANGE SPRING STATES

Before embarking on an examination of the experimental results it is instructive to appreciate just how the inclusion of small amounts of Er into a YFe_2 dominated $DyFe_2/YFe_2$ spring system increases complexity. There is a substantial increase in the number of exchange spring states.

In Fig. 1 we show the calculated anisotropy surfaces of the Er^{3+} and Dy^{3+} rare earth ions at 100 K. These surfaces were obtained using the modified Callen and Callen model [20,21]. It is immediately apparent that the Er and Dy ions are characterized by ⟨001⟩ and ⟨111⟩ easy axes of magnetization, respectively. Consequently, the introduction of sufficient numbers of Er ions into the soft YFe_2 layers of nominally $DyFe_2/YFe_2$ multilayers has the potential to create noncollinear magnetic exchange spring states, even in zero field.

Figure 2 shows two exchange spring spin states, both stable in zero field. These states are characterized by Dy moments pointing along an in-plane [001] axis, while the Er is either in-plane or out-of-plane. In the absence of strain and/or demagnetization effects both the spin systems shown in Fig. 2 possess the same energy. However, the two spin states depicted

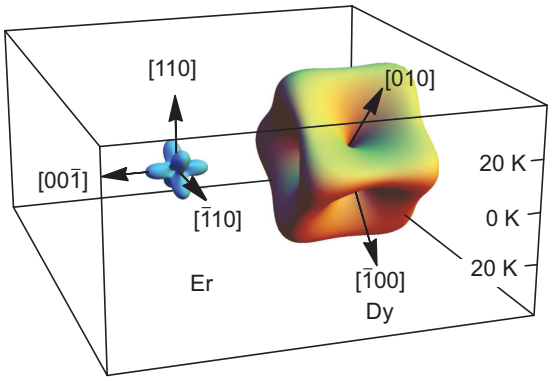

FIG. 1. (Color online) Anisotropy energy surfaces for Er^{3+} and Dy^{3+} ions in the cubic Laves RFe_2 compounds at 100 K. Note that the Er moments can easily change direction, between easy ⟨111⟩ directions, by sliding over low energy saddle ⟨110⟩ points. By contrast, the Dy moments have to jump over quite a large energy barrier.

in Fig. 2 are not unique. Altogether there are eight spin states, all essentially with the same energy, as listed in Table II of Appendix A.

In addition to the states shown in Fig. 2 and listed in Table II, there are other spring states available to the system. Two alternative spin states can be seen in Fig. 3. Note that this time the Dy moments are pointing out-of-plane, while the Er can be either in-plane or out-of-plane. Once again the two spin

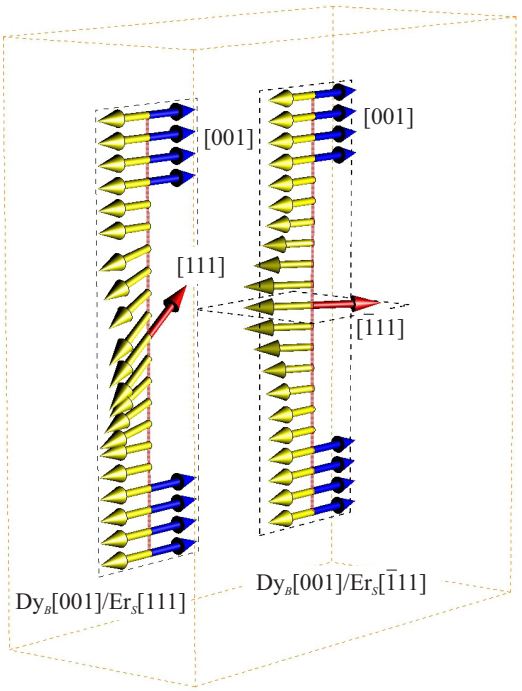

FIG. 2. (Color online) Schematic representations of two stable exchange spring states in zero field. The blue (red) arrows represent the Dy (Er) moments, respectively, while the yellow arrows represent the Fe moments. We denote these two spin configurations as $Dy_B[001]/Er_S[111]$ (left) and $Dy_B[001]/Er_S[\bar{1}11]$ (right), respectively. Here the Dy_B (Er_S) stands for the bulk Dy (Er in the spring), respectively. Note that the precise direction of the Er moments will be modified by the presence of exchange springs.

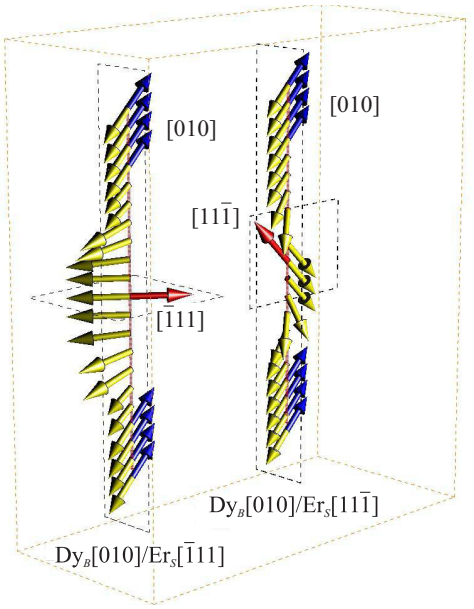

FIG. 3. (Color online) Schematic representations of two stable exchange spring states in zero field. Notation and color scheme as per Fig. 2. We denote these two exchange spring states as $Dy_B[010]/Er_S[\bar{1}11]$ (left) and $Dy_B[010]/Er_S[11\bar{1}]$ (right), respectively.

states depicted in Fig. 3 are not the only spring states available to the system. Equivalent spin states, in the absence of strain, are summarized in Table III of Appendix A.

In all, there would appear to be 24 different spin systems characterized by either true or local minima in zero field. It is also obvious, from an examination of Figs. 2 and 3, that in general, the spin configurations are not easily classified simply in terms of either Bloch (in-plane/out-of-plane/in-plane) or Néel (all in-plane) domain walls. In general they are mixed. In the case of Fig. 2, the two states $Dy_B[001]/Er_S[111]$ (Dy_B $[001]/Er_S$ $[\bar{1}11]$) could be described as Bloch wall (Néel wall), respectively, with the proviso that the two domain walls are far from 180°. However, in the case of Fig. 3, it is clear that the two states do not fall easily into either Bloch- or Néel-wall classification.

Finally, as noted earlier, the Er moments are likely to be disturbed from their ⟨111⟩ easy axes. Thus care must be exercised when assigning spring states to selected regions of the M versus B_a magnetization loop. As we shall see the magnetization loop of the Dy sublattice, as revealed by Dy-XMCD, is far from trivial.

III. EXPERIMENTAL DETAILS

$[DyFe_2\,(60\,Å)/YFe_2\,(120\,Å)/ErFe_2\,(8\,Å)/YFe_2\,(120\,Å)]_{15}$ was grown by molecular beam epitaxy (MBE) [22,23]. Briefly, a 100-Å-thick Nb buffer layer followed by a 20 Å Fe seed layer were first deposited onto an epiready $(11\bar{2}0)$ sapphire substrate. The Laves phase material was subsequently grown in (110) orientation, with the major axes parallel to those of Nb. This was achieved by codeposition of elemental fluxes at a substrate temperature of 600 °C. Finally, to prevent oxidation the multilayer was capped with 10 nm of Nb.

For the XMCD experiments it is not possible to have the x-ray beam directly along an easy [001] in-plane axis. In practice,

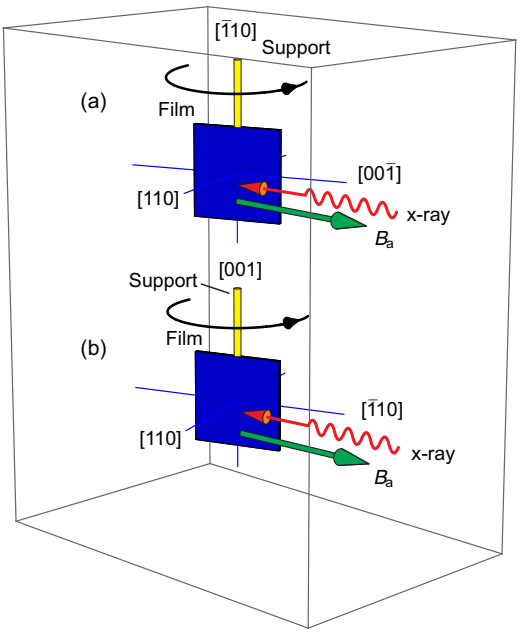

FIG. 4. (Color online) Geometry used in the XMCD experiments. In (a) and (b) the x-ray beam is directed along an easy [001] and hard [$\bar{1}$10] axis, respectively. The magnetic field and the x-ray beam are collinear, and the film can be rotated either way about the vertical (support) axis.

it is necessary to rotate the sample about the vertical axis by 10° to allow the x-ray beam to strike the film surface at grazing incidence. The situation is sketched in Fig. 4(a). In the second set of experiments the x-ray beam and the applied magnetic field were directed essentially along a hard [$\bar{1}$10] in-plane axis, as sketched in Fig. 4(b). In both types of experiments the x-ray beam and the applied magnetic field are collinear.

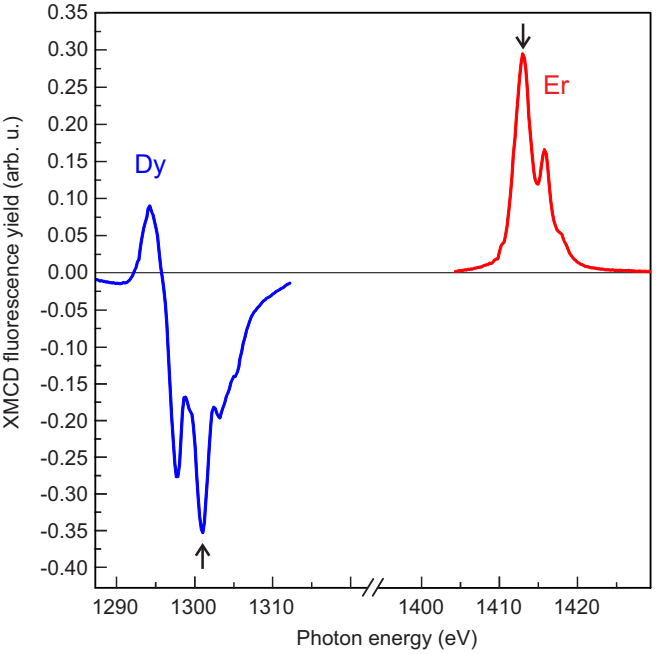

FIG. 5. (Color online) Dy- and Er-XMCD signals measured using fluorescence yield.

The XMCD experiments were performed at the Dy M_5 (1301 eV) and Er M_5 (1413 eV) absorption edges [24]. Typical Dy- and Er-XMCD signals can be seen in Fig. 5. The arrows indicate the photon energies used to trace the magnetization loops.

The spectra were obtained using two fluorescence detectors, parallel and perpendicular to the incoming x rays. Finally, the temperature of the sample could be varied between 4 and 300 K, while the magnetic field could be swept from 0 to ± 14 T. However, for the measurements reported here, the temperature was set at 100 K. At this temperature it is well known that the Dy easy axis lies in-plane, along a [001] axis [13,14]. Moreover, the choice of this temperature guarantees that full loops can be obtained. It also allows easy comparison with earlier results on undoped and Dy-doped samples [15,18].

IV. EXPERIMENTAL RESULTS

The Dy- and Er-XMCD magnetization curves obtained using the magnetic field directed along an easy in-plane Dy [001] axis and a hard in-plane [$\bar{1}$10] axis can be seen in Figs. 6 and 7, respectively. Also included in the diagrams is the first derivative of the Dy loop, ($\partial M_{\mathrm{Dy}}/\partial B_{\mathrm{a}}$). The dotted lines in both figures show the maxima of the first derivative where the pace of change between the various exchange spring states is most rapid. However, the minima in the first derivative signify those field regions where the states are "stable."

The first point to note is that the magnetization curves for fields applied along a Dy easy (hard) axis [001] ([$\bar{1}$10]),

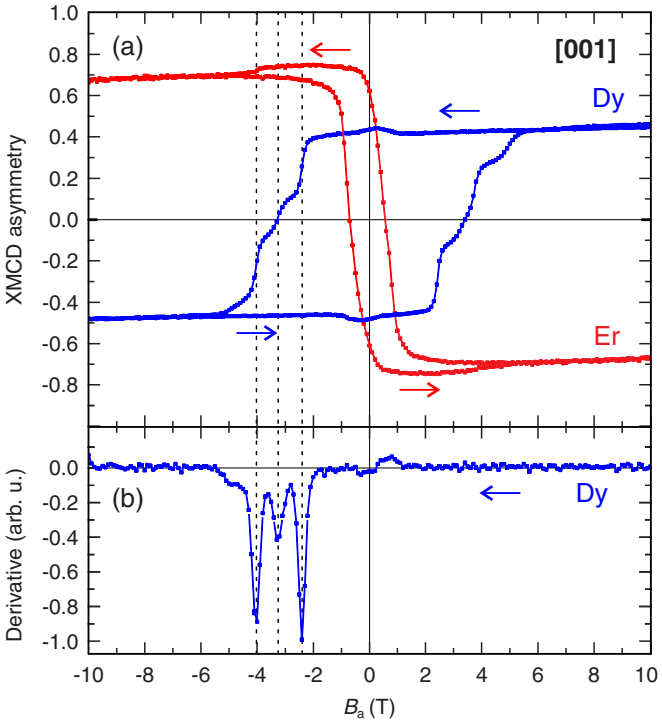

FIG. 6. (Color online) (a) Dy (blue) and Er (red) element-specific XMCD-magnetization loops for magnetic fields applied along an in-plane [001] axis. (b) First derivative $\partial M_{\mathrm{Dy}}/\partial B_{\mathrm{a}}$ for decreasing applied field. The derivative for increasing field is essentially the same, but inverted in signal and field.

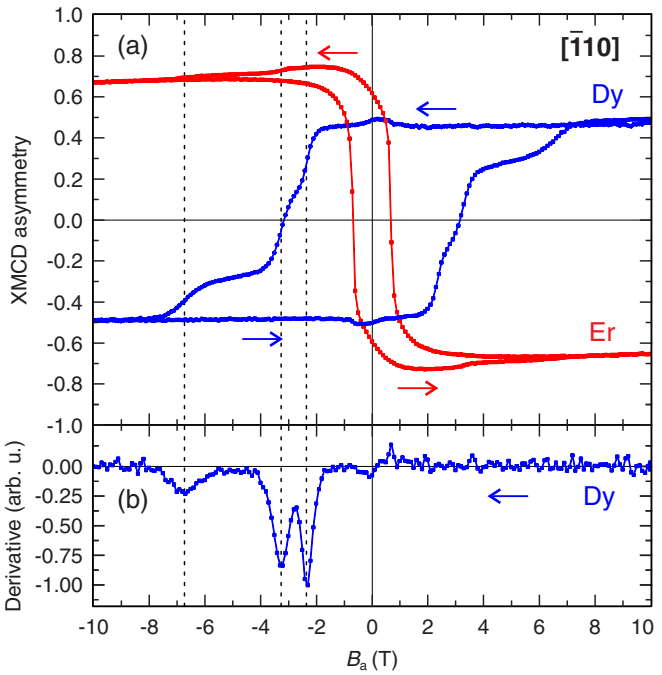

FIG. 7. (Color online) (a) Dy (blue) and Er (red) element-specific XMCD-magnetization loops for magnetic fields applied along an in-plane [$\bar{1}$10] axis. (b) First derivative $\partial M_{\mathrm{Dy}}/\partial B_{\mathrm{a}}$ for decreasing applied field.

respectively, appear to be very similar to each other. However, the reader is warned that the spin configurations involved in these two cases are very different. This problem was first addressed in Ref. [17], where it was shown that for a [$DyFe_2$ (60 Å)/YFe_2 (240 Å)] multilayer (no doping) the [001] ([$\bar{1}$10]) magnetization curves are characterized by Dy moments being in-plane (out-of-plane), respectively. Schematic spin configurations illustrating these two cases can be seen in Fig. 3 of Ref. [17]. They bear some resemblance to those shown in Figs. 2 and 3 of this paper, but the presence of the Er brings about substantial changes. Finally, as already noted, the magnetic reversal of the undoped [$DyFe_2$ (60 Å)/YFe_2 (240 Å)] multilayer involves both in-plane and out-of-plane *transverse* exchange spring states [15,16]. Consequently, both in-plane and out-of-plane states can be anticipated, as the Er-doped multilayer is taken around its M-B_a loop.

In Sec. VI and Appendix C we present possible magnetic reversal scenarios for magnetic fields applied along an easy in-plane [00$\bar{1}$] axis and hard in-plane [$\bar{1}$10] axis, respectively. Our interpretations are based on (*i*) the experimental data, both full and partial loops, and (*ii*) predictions obtained using micromagnetic modeling. The latter is briefly described in Sec. V.

V. MAGNETIC MODELING

The model used in this work has been previously described in Ref. [25]. Briefly, the cubic Laves $R\mathrm{Fe}_2$ compounds are characterized by a strong ferromagnetic (FM) Fe-Fe exchange B_{ex}(Fe-Fe) ≈ 600 K, which runs throughout the entire lattice. This interaction is primarily responsible for the high Curie temperatures. Next, in magnitude, is the AF

Dy-Fe and Er-Fe exchange fields B_{ex}(Dy-Fe) $\approx$ 100 K and B_{ex}(Er-Fe) $\approx$ 80 K (all estimates at $T = 0$ K). Here we adopt a four component magnetic model, with the Dy, Er, Y, and Fe magnetic moments set at 10 μ_B, 9 μ_B, $\sim$0 μ_B, and 1.5 μ_B, respectively (again at $T = 0$ K) [26]. At 100 K these moments are temperature-adjusted to $10 \times 0.9203\,\mu_B$, $9 \times 0.8344\,\mu_B$, $\sim 0\,\mu_B$, and $1.5 \times 0.9835\,\mu_B$, respectively. Of course, the model is a gross oversimplification. For example, band-structure calculations reveal that there are induced R 5d moments, in addition to the Fe 3d moments [27]. However, given that the 5d moments are driven primarily by the Fe 3d sublattice, it is a reasonable approximation to use a discrete two-component R-Fe model, provided we ascribe say $\mu_{Dy} = 10\,\mu_B$ and $\mu_{Fe}(=\mu_{3d} + \mu_{5d}) = 1.5\,\mu_B$ [26]. Also, in addition to magnetic exchange and moments, estimates for both the Dy and Er cubic anisotropy and strain parameters are also required. The latter have been taken from Refs. [20,21]. Indeed, this data has already been used to compute the anisotropy surfaces shown in Fig. 1.

Finally, as noted in Ref. [18], it is not possible to model the many steps encountered in the reversible mechanism, accurately. For example, small changes in the many parameters used in the model can lead to differing magnetic reversal mechanisms. Consequently, in practice, it is best to use the results of the micromagnetic model as a guide to the interpretation of the full and partial loops presented in Sec. VI and Appendix C below. However, the interested reader can find many of the model predictions further in the Appendixes B and D.

VI. FIELD APPLIED ALONG AN EASY IN-PLANE [00$\bar{1}$] AXIS

First, we note that there are four possibilities for the ground state in a high magnetic field applied along the [00$\bar{1}$] axis. These are (*i*) the two equivalent Dy in-plane/Er in-plane states $Dy_B[00\bar{1}]/Er_S[\bar{1}11]$ and $Dy_B[00\bar{1}]/Er_S[1\bar{1}1]$ and (*ii*) the two equivalent Dy in-plane/Er out-of-plane states $Dy_B[00\bar{1}]/Er_S[111]$ and $Dy_B[00\bar{1}]/Er_S[\bar{1}\bar{1}1]$. In order to decide between these two possibilities we turn to the micromagnetic model described in more detail in Ref. [25]. The calculated Stoner-Wohlfarth limits for the various spin states are summarized in Table I.

From an examination of Table I it will be seen that there are eight possible spin configurations available to the system.

TABLE I. Some calculated Stoner-Wohlfarth limits obtained using the micromagnetic model described in Ref. [25], for fields applied along an easy [00$\bar{1}$] axis.

Spin system	Stoner-Wohlfarth limits (T)
$Dy_B[00\bar{1}]/Er_S[\bar{1}11]$	$0.3661 \leqslant B_a < (50+)$
$Dy_B[00\bar{1}]/Er_S[111]$	$0.4076 \leqslant B_a \leqslant 3.526$
$Dy_B[00\bar{1}]/Er_S[11\bar{1}]$	$-51.10 \leqslant B_a \leqslant 0.9351$
$Dy_B[00\bar{1}]/Er_S[\bar{1}\bar{1}\bar{1}]$	$-51.10 \leqslant B_a \leqslant 9.651$
$Dy_B[010]/Er_S[\bar{1}11]$	$-0.2920 \leqslant B_a \leqslant 18.75$
$Dy_B[010]/Er_S[\bar{1}\bar{1}\bar{1}]$	$-18.75 \leqslant B_a \leqslant 0.2920$
$Dy_B[010]/Er_S[11\bar{1}]$	$-18.75 \leqslant B_a \leqslant 0.2604$
$Dy_B[010]/Er_S[111]$	$-0.2604 \leqslant B_a \leqslant 18.75$

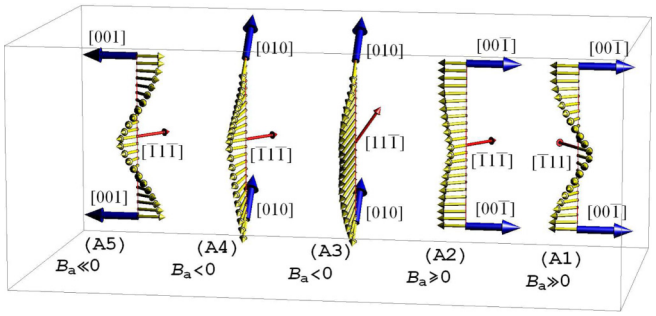

FIG. 8. (Color online) Plausible four-step magnetic reversal process in an Er-doped $DyFe_2/YFe_2$ multilayer, for fields directed along an in-plane easy [00$\bar{1}$] axis. The proposed spin state sequence is only valid starting from a large positive field state (A1) and reducing to a large negative field state (A5).

There are more, but they are related by symmetry to those of Table I. More details of their properties, energy, magnetic moments, etc., of some of the states are summarized in Appendix B. For present purposes we note that in a high magnetic field only the *all* in-plane Néel state $Dy_B[00\bar{1}]/Er_S[\bar{1}11]$ (top row of Table I) is stable. This state is depicted schematically by (A1) in the magnetic reversal scenario of Fig. 8.

Using Fig. 8, we can describe the magnetic reversal mechanism as follows.

(1) As the magnetic field is reduced the exchange springs unwind, reversibly, in-plane. However, eventually the Er moments in the middle of the spring will come up against a hard in-plane [$\bar{1}$10] axis which resists further unwinding. Consequently, a critical field will be reached where the Er magnetic moments become unstable and suddenly switch to a new easy in-plane [$\bar{1}1\bar{1}$] axis. We refer to this irreversible process as *exchange-spring collapse*. Note that during this process, the Dy moments remain essentially unchanged still pointing along the [00$\bar{1}$] axis. Indeed, the Stoner-Wohlfarth limits for the (A1) spin configuration are $0.37 \leqslant B_a \leqslant (50+)$ T. So the micromagnetic model predicts that the Er must switch in a small positive field.

(2) As the field is reduced still further to negative values, we know from earlier studies on undoped $DyFe_2/YFe_2$ multilayers that the reversal mechanism involves the Dy moments switching from in-plane [00$\bar{1}$] to an out-of-plane $\langle 010 \rangle$ axis [15,16]. In the present situation, there are two possibilities: the all in-plane states $Dy_B[010]/Er_S[\bar{1}1\bar{1}]$ and $Dy_B[010]/Er_S[11\bar{1}]$, with the Stoner-Wohlfarth limits $-18.764 \leqslant B_a \leqslant 0.292$ T and $-18.764 \leqslant B_a \leqslant 0.260$ T, respectively. We believe that the most likely candidate is the $Dy_B[010]/Er_S[11\bar{1}]$ state, depicted by (A3) in Fig. 8. Here the Er is now out-of-plane, but still with a component along the [00$\bar{1}$] axis, nominally equal to that of state (A2). Note that this state has all its moments pointing out-of-plane, i.e., a Bloch-like wall.

(3) On reducing the field still further, the Er switches back into plane, from a [11$\bar{1}$] to [$\bar{1}1\bar{1}$] axis, while leaving the Dy moment unchanged. This gives rise to the $Dy_B[010]/Er_S[\bar{1}1\bar{1}]$ state, depicted by (A4) in Fig. 8.

(4) Finally, in a large negative field the Dy moment switches to the easy [001] axis, leaving the Er moment essentially

unchanged. This gives rise to the negative high-field state $Dy_B[001]/Er_S[\bar{1}1\bar{1}]$ (A5), the reverse of (A1).

Quite apart from calculations, we have also experimental evidence for the reversal mechanism shown schematically in Fig. 8. In the first place, we note that on switching from state (A1) to (A2) the Dy-XMCD signal remained essentially unchanged, while the Er-XMCD signal undergoes a dramatic switch from negative to positive. These observations are in accord with the experimental data of Fig. 6. Secondly, when the Dy moments are out-of-plane axis, at right angles to the applied magnetic field, the Dy-XMCD signal should vanish. In the present case of the Er-doped multilayer, the Dy-XMCD signal near zero shows the presence of two distinct states at −2.84 T and −3.6 T. We assign these the two states to (A3) and (A4), respectively, as depicted in Fig. 8.

Further evidence for the four step mechanism shown in Fig. 8 can be gleaned from the partial loops shown in Figs. 9(a) and 9(b). When the field is cycled from $+10 \rightarrow -2.84 \rightarrow +10$ T the Er loop shown in Fig. 9(a) is, to all intents and purposes, reversible. At first sight this is surprising, given that the Er switch in going from (A1) to (A2) is irreversible (exchange spring collapse). However, as mentioned earlier the Er moments can easily slide over a shallow saddle points, in this case the $[\bar{1}10]$ axis

Similarly, when the field is cycled from $+10$ T $\rightarrow -3.6$ T [Fig. 9(b)] we see that although the Er is loop is not fully reversible, the magnitude of the Er-XMCD signal is practically the same. This too is consistent with cycling between the (A1) and (A4) states. Likewise, accompanying changes in the Dy-XMCD signal have to be large, given that the Dy moments cycle between the $[00\bar{1}] \rightarrow [010] \rightarrow [00\bar{1}]$ axes.

In summary, it is clear that the two *transverse* states (A3) and (A4) are not identical. We ascribe the difference in the two Dy-XMCD signals as due to (*i*) the increase in magnetic field, in going from (A3) to (A4), pulling the Dy moments ever closer towards the final [001] direction, and (*ii*) differences in the nominally Dy [010] direction, caused by Er moments on switching between the $[11\bar{1}]$ and $[\bar{1}1\bar{1}]$ axes, respectively. A discussion of the reversal for fields applied along a hard axis can be found in Appendix C.

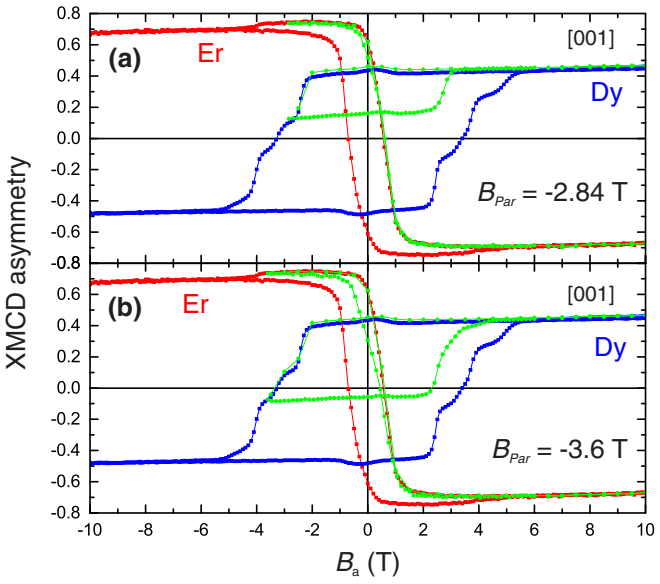

FIG. 9. (Color online) Partial loop (green) obtained by sweeping the field from (a) $10 \rightarrow -2.84 \rightarrow 10$ T and (b) from $10 \rightarrow -3.6 \rightarrow 10$ T, for a magnetic field applied along an in-plane [001] axis.

VII. SIMPLE EXPLANATION OF EXCHANGE SPRING COLLAPSE

To simplify matters, we shall ignore the Dy out-of-plane *transverse* exchange springs (A3) and (A4). In short, we use the micromagnetic model to calculate the Dy and Er loops, for the simple two step reversal mechanism:

$$Dy_B[00\bar{1}]/Er_S[\bar{1}11] \rightarrow Dy_B[00\bar{1}]/Er_S[\bar{1}1\bar{1}] \rightarrow Dy_B[001]Er_S[\bar{1}1\bar{1}]$$

The results of this calculation can be seen in Fig. 10.

It will be observed that even this simplistic interpretation replicates the experimental data of Fig. 6 reasonably well. Here the Dy loop is conventional, i.e., positive moments in positive fields, while the Er loop is unconventional in that the loop appears to be the wrong way around. The underlying reason for this behavior is easy to understand. The Er is in the center of the YFe_2 layer. So the direction of the Er moments is dictated by that of the exchange spring present in the YFe_2 layer. In large applied fields, the Fe moments in the $DyFe_2$ and YFe_2 layers are essentially antiparallel to each other. Consequently, the components of the Dy and Er moments, in the direction of the x-ray beam, must be roughly antiparallel too, in accord with (A1) of Fig. 8. Thus the corresponding Er signal, for a large positive Dy-XMCD signal, must be negative. However, as the magnetic field is reduced to zero, the exchange spring will unwind, eventually collapsing, leading a near net AF state (A2) where the components of the Dy and Er moments along the x-ray beam are roughly parallel. Here the sign of the Er-XMCD signal is now positive.

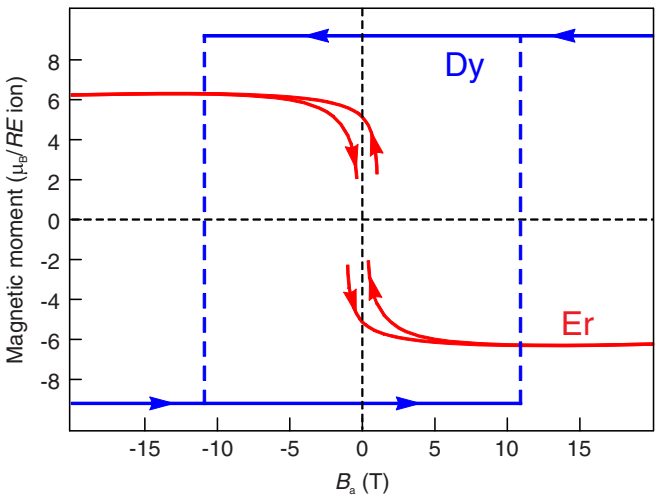

FIG. 10. (Color online) Calculated Dy and Er loops at 100 K for a two-step magnetic reversal: $Dy_B[00\bar{1}]/Er_S[\bar{1}11] \rightarrow Dy_B[00\bar{1}]/Er_S[\bar{1}1\bar{1}] \rightarrow Dy_B[001]/Er_S[\bar{1}1\bar{1}]$. Red curve Er; blue curve Dy.

From an examination of Fig. 10, it is clear that the loop is characterized by two very different coercivities, with that of the Er loop being much smaller than that of the Dy loop. This too is relatively easy to understand. In the first place, the inherent anisotropy of the Dy ions is stronger than that of the Er (see Fig. 1). Secondly, the number of Dy ions outweighs the Er by a factor of 15:2. Thirdly, and most importantly, the "anisotropy" of the Er loop is dictated by its low energy saddle $\langle 110 \rangle$ points, as illustrated in Fig. 1. Consequently, the coercive field of the Er loop is dictated primarily by the bending-field of the exchange spring.

Next we detail how we have estimated the "coercivity" of the Dy sublattice shown in Fig. 10, namely $B_C = 10.9$ T. Following Refs. [18,25] we first calculate the equivalent Stoner Wohlfarth limits for Dy reversal. From Table I we find that the state $Dy_B[00\bar{1}]/Er_S[\bar{1}1\bar{1}]$ becomes unstable at -55.1 T. However, the energy of the reversed state $Dy_B[001]/Er_S[\bar{1}1\bar{1}]$ dips below that of $Dy_B[00\bar{1}]/Er_S[\bar{1}1\bar{1}]$ at -2.15 T. In practice, of course, the actual Dy switching field must lie somewhere between these two limits $B_{CO} \leqslant B_C \leqslant B_{SW}$. Thus following Ref. [25] we estimate the coercive field of the Dy using the geometric mean $B_C = \sqrt{B_{SW} B_{CO}} = 10.9$ T. This value is in excess of the measured coercivity by about a factor of 2.2, but it is a better estimate than that afforded by the Stoner-Wohlfarth method.

In practice, of course, the overall switching mechanism is obviously more complex, involving both in-plane and transverse magnetic exchange spring states, as detailed in Figs. 8 and 13. Nevertheless, the essential physics of the exchange spring collapse, and the two element selective loops with very different coercive fields, will remain.

Finally, we note from experiment (see Figs. 6 and 7) that the phenomenon of exchange spring collapse is much sharper for the $[\bar{1}10]$ direction than it is for the [001] axis.

VIII. COMPARISON BETWEEN Er- AND Dy-DOPED SAMPLES

It is instructive to compare results obtained earlier for the Dy-doped multilayers [18], with that of the Er-doped films discussed in this work. A comparison of both the Dy and Er-doped samples, for fields applied along a hard $[\bar{1}10]$ axis, can be seen in Fig. 11.

In the case of the Dy-doped sample, the reversal of the Dy moment in the spring at $B_a = 0.5$ T gives rise to just a small step in the Dy-XMCD signal. This is because 8 Å of Dy in the spring only contributes ~13% to the total Dy signal. By contrast, reversal of the Er moment in the spring at $B_a = 1$ T results in a huge signal, swinging from a large negative to a large positive value. Thus in the study of doped-exchange spring systems the use of element-selective XMCD confers significant advantages, provided the element in spring differs from that in the bulk.

IX. DISCUSSION AND CONCLUSIONS

In this paper it has been shown that placing small quantities of $ErFe_2$, directly into the center of the soft YFe_2 layers in multilayer $DyFe_2/YFe_2$, brings about substantial changes. In short, because of the differing directions of easy magnetization

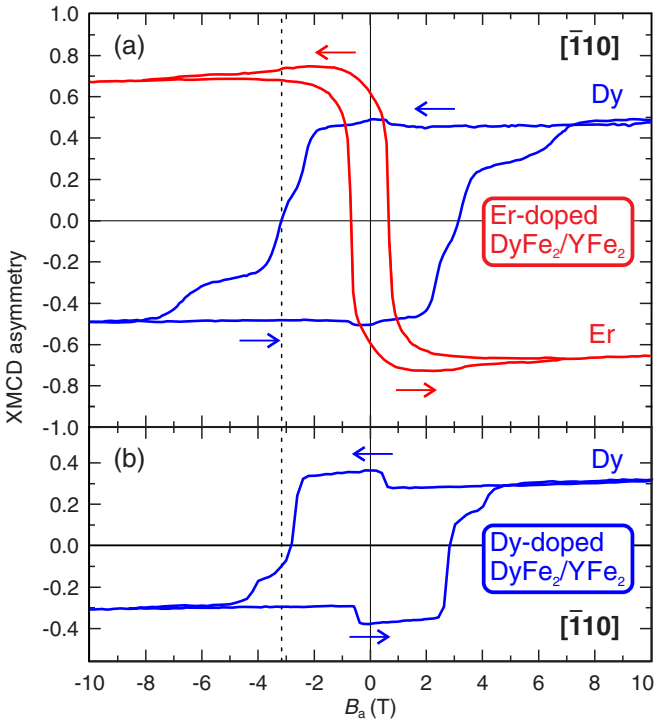

FIG. 11. (Color online) Comparison between the (a) Er- and (b) Dy-doped $DyFe_2/YFe_2$ multilayers at 100 K for fields applied along a hard in-plane $[\bar{1}10]$ axis.

for the Dy^{3+} and Er^{3+} moments, there is a substantial increase in the number of spring states available to the system. As a result, the Er-doped $DyFe_2/YFe_2$ multilayer is now characterized by noncollinear exchange springs, even in zero field. Furthermore, pinning of the soft YFe_2 layers by the Er^{3+} ions gives rise to the phenomenon of exchange spring collapse. This is evident from the Dy- and Er-XMCD loops which clearly show two differing switching fields for the two elements in question. The experimental XMCD results have also been complemented with micromagnetic modeling. In particular, the latter has been used to provide a reasonable explanation of the two strikingly different Dy and Er magnetization loops. Finally, loops for the Dy sublattice (both full and partial) show that at least 10 different exchange spring states are accessed during magnetic reversal, for fields applied along an in-plane easy $[00\bar{1}]$ axis/hard $[\bar{1}10]$ axis, respectively. In general, these states are not easily classified in terms of Néel/Bloch domain walls. In particular, they cannot be described simply as 180° walls.

It is also evident, from the results obtained during this work, that ~8 Å of $ErFe_2$ is sufficient to pin the middle of the exchange spring along near $\langle 111 \rangle$-type axes. However, if the Er content is reduced still further, there will be a situation where the physics will change. For very dilute Er^{3+} doping, the role played by the Er anisotropy will diminish and the Er moments will simply follow the moments in the YFe_2 layers. In such cases, the Er XMCD signal could then be used as a "spy" in the YFe_2 spring. In practice, we have found that very reasonable Er-XMCD signals can be obtained with just 8-Å-thick layers of $ErFe_2$. Thus it is reasonable to expect that excellent signal

to noise Er-XMCD signals will be obtained with just a tenth of the Er doping used in this work. Consequently, it should be possible to determine that level of Er doping at which the four-step magnetic reversal identified in this work reverts to the two-step process present in the undoped system [16]. By contrast, such experiments would be very difficult to perform using dilute Dy doping. Here the Dy-XMCD signal from inside the exchange spring would be totally swamped by that from the block Dy [18] (see also Fig. 11).

Finally, in passing it is worth making two points. First, the $DyFe_2/YFe_2$ system discussed in this work has been used to demonstrate giant magnetoresistance (GMR) [19]. Here the GMR has been linked explicitly to the "curvature" of the exchange spring in the YFe_2 layers, in applied magnetic fields. Thus it would be of interest to measure the GMR of doped exchange spring systems, where the presence of doped layers provides an additional scattering mechanism. Secondly, the Er-XMCD signal clearly demonstrates that very low levels of RE-doping can be examined using XMCD. Thus it might be possible to grow exchange spring systems doped with light—as opposed to heavy—rare earth elements. In general, rare earth Laves compounds, such as $PrFe_2$ and $NdFe_2$, can only be grown at very high temperatures and pressures [28]. However, at very low doping levels it might be possible to incorporate light rare earths into the YFe_2 layers. If this can be done, the GMR of nanometer-thick films could be examined with both ferromagnetic and antiferromagnetic coupling, between the Fe and the R moments in question.

ACKNOWLEDGMENTS

We acknowledge Diamond Light Source for time on beamline I10 under proposal SI-8213, and Keith Belcher for help with the MBE growth.

APPENDIX A: TABLES OF THE EXCHANGE SPRING STATES AVAILABLE TO THE Er-DOPED $DyFe_2/YFe_2$ MULTILAYER

There are numerous spin-states available to the Er-doped $DyFe_2/YFe_2$ multilayer. Here we summarize the Dy in-plane (Table II) and out-of-plane (Table III) exchange spring states at 100 K in zero applied field.

TABLE II. Summary of Dy in-plane spring states available to Dy/Er spring system in zero field [in-plane means the (110) plane]. For all states the angle between the Dy and Er moments is $\arccos(1/\sqrt{3}) = 54.7^\circ$, but this angle will be modified by the exchange springs, strain, demagnetization, and applied magnetic fields.

Dy in-plane Er in-plane	Dy in-plane Er out-of-plane
$Dy_B[001]/Er_S[\bar{1}11]$	$Dy_B[001]/Er_S[111]$
$Dy_B[001]/Er_S[1\bar{1}1]$	$Dy_B[001]/Er_S[\bar{1}\bar{1}1]$
$Dy_B[00\bar{1}]/Er_S[\bar{1}1\bar{1}]$	$Dy_B[00\bar{1}]/Er_S[11\bar{1}]$
$Dy_B[00\bar{1}]/Er_S[1\bar{1}\bar{1}]$	$Dy_B[00\bar{1}]/Er_S[\bar{1}\bar{1}\bar{1}]$

TABLE III. Summary of Dy out-of-plane spring states available to Dy/Er spring system in zero field. In the absence of strain and demagnetization, these states possess the same energy in zero field.

Dy out-of-plane Er in-plane	Dy out-of-plane Er out-of-plane
$Dy_B[010]/Er_S[\bar{1}1\bar{1}]$	$Dy_B[010]/Er_S[111]$
$Dy_B[010]/Er_S[\bar{1}11]$	$Dy_B[010]/Er_S[11\bar{1}]$
$Dy_B[0\bar{1}0]/Er_S[1\bar{1}1]$	$Dy_B[0\bar{1}0]/Er_S[\bar{1}\bar{1}\bar{1}]$
$Dy_B[0\bar{1}0]/Er_S[1\bar{1}\bar{1}]$	$Dy_B[0\bar{1}0]/Er_S[\bar{1}\bar{1}1]$
$Dy_B[100]/Er_S[1\bar{1}\bar{1}]$	$Dy_B[100]/Er_S[111]$
$Dy_B[100]/Er_S[1\bar{1}1]$	$Dy_B[100]/Er_S[11\bar{1}]$
$Dy_B[\bar{1}00]/Er_S[\bar{1}1\bar{1}]$	$Dy_B[\bar{1}00]/Er_S[\bar{1}\bar{1}1]$
$Dy_B[\bar{1}00]/Er_S[\bar{1}11]$	$Dy_B[\bar{1}00]/Er_S[\bar{1}\bar{1}1]$

APPENDIX B: DIAGRAMS FOR THE [00$\bar{1}$] LOOP

From an examination of the energies of the (A1) → (A4) spring states shown in Fig. 12(a) it is clear that the in-plane state (A1) ($Dy_B[00\bar{1}]/Er_S[\bar{1}11]$) possesses the lowest energy in a large positive magnetic field. However, as the field is reduced to near zero, exchange spring collapse occurs and the spin-state morphs into the near AF state (A2). This state is surprisingly stable out to a negative field of some −20 T. However, it has a higher energy than those of the out-of-plane states (A3) and (A4). Thus a transition to the lower (A3) and (A4) states must occur as the field is taken towards more negative values. What is surprising about Fig. 12(a) is the near equivalence of the energies of spin states (A3) and (A4). Rather surprisingly, this is also true for their overall magnetic moments [see Fig. 12(b)], and the Dy and Er moments [see Figs. 12(c) and 12(d)]. However, their Stoner-Wohlfarth field ranges differ slightly (see Table I).

APPENDIX C: FIELD APPLIED ALONG A HARD IN-PLANE [$\bar{1}$10] AXIS

Magnetic reversal for fields applied along a hard [$\bar{1}$10] axis in an undoped $DyFe_2/YFe_2$ multilayer has been previously discussed in Ref. [17]. These authors interpreted the bulk magnetization loop in terms of a simple switch from one out-of-plane axis to another on the opposite side of the film. However, in the case of the Er-doped multilayer, it is clear from Fig. 7 that at least four steps are involved. The spin states identified using micromagnetic modeling can be seen in Table IV, along with their Stoner-Wohlfarth limits. Once again,

TABLE IV. Spin states for fields applied along a hard [$\bar{1}$10] axis with their calculated Stoner-Wohlfarth limits.

Spin system	Stoner-Wohlfarth limits (T)
$Dy_B[010]/Er_S[1\bar{1}\bar{1}]$	$0.5471 \leqslant B_y < (50+)$
$Dy_B[010]/Er_S[\bar{1}1\bar{1}]$	$-21.93 \leqslant B_y \leqslant 0.3858$
$Dy_B[010]/Er_S[11\bar{1}]$	$-0.4343 \leqslant B_y \leqslant 1.214$
$Dy_B[00\bar{1}]/Er_S[1\bar{1}\bar{1}]$	$-0.4374 \leqslant B_y \leqslant 17.54$
$Dy_B[00\bar{1}]/Er_S[\bar{1}1\bar{1}]$	$-17.54 \leqslant B_y \leqslant 0.4374$
$Dy_B[00\bar{1}]/Er_S[11\bar{1}]$	$-0.04251 \leqslant B_y \leqslant 0.4251$

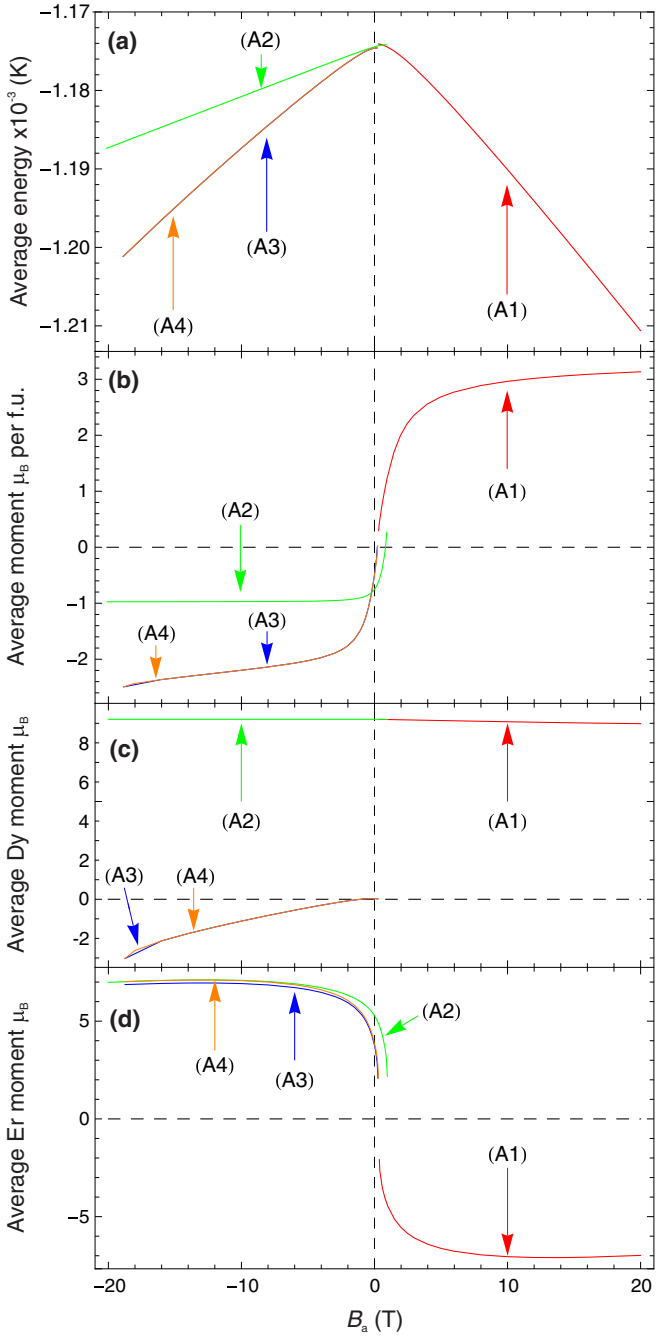

FIG. 12. (Color online) (a) Average energy per formula unit vs magnetic field, (b) average moment per formula unit vs magnetic field, (c) average Dy moment vs magnetic field, and (d) average Er moment vs magnetic field for the first four states (A1) → (A4) of Fig. 8.

more details concerning the predictions of the micromagnetic model can be found in Appendix D.

Using Table IV, and Appendix D, we suggest the plausible four-step switching mechanism shown in Fig. 13.

With the aid of Fig. 13 we describe the magnetic reversal mechanism as follows.

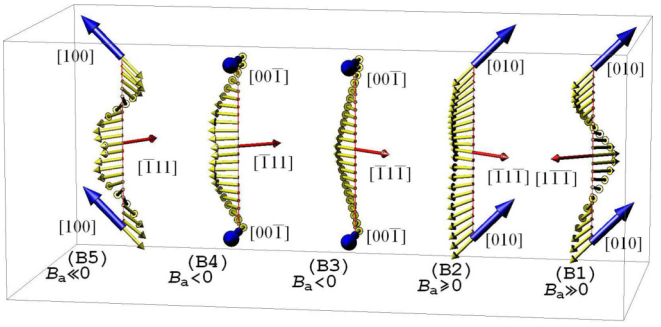

FIG. 13. (Color online) Plausible four-step magnetic reversal process in a Er-doped $DyFe_2/YFe_2$ multilayer, for fields directed along a hard in-plane $[\bar{1}10]$ axis. The proposed spin state sequence is only valid starting from a large positive field state (B1), reducing to a large negative field state (B5).

(1) We start with the saturated state (B1), i.e., $Dy_B[010]/Er_S[1\bar{1}\bar{1}]$, Dy out-of-plane, Er in-plane. Here the components of the Dy and Er moments in the direction of the x-ray beam are roughly antiparallel. As a result, a large Fe-Fe exchange spring is present in the soft YFe_2 layer.

(2) At say $B_a = +1$ T, exchange spring collapse occurs (B1) → (B2). By $B_a = -1$ T, the Er switch is complete. The state can then be described as $Dy_B[010]/Er_S[\bar{1}1\bar{1}]$. In short, the Er moments switch but the Dy moments do not. Thus we see a large change in the Er-XMCD signal, but almost nothing in the Dy-XMCD signal, in agreement with the experimental results of Fig. 7.

(3) At $B_a = -2.75$ T, (B2) → (B3). Here the Dy switches to an in-plane $[00\bar{1}]$ axis almost transverse to the applied magnetic field, leaving the Er moments essentially unchanged: $Dy_B[00\bar{1}]/Er_S[\bar{1}1\bar{1}]$. Thus there is a large change in the Dy-XMCD but not much in the Er signal.

(4) At $B_a = -5$ T, (B3) → (B4). The Er moments flip from $[\bar{1}1\bar{1}]$ to the $[\bar{1}11]$ axis, leaving the Dy moments essentially changed, i.e., the $Dy_B[00\bar{1}]/Er_S[\bar{1}11]$ state. This Er flip will not bring about much change in the Er-XMCD signal. Note that (B3) and (B4) could be described as in-plane Néel walls.

(5) Finally, at $B_a = -7.5$ T, (B4) → (B5). The Dy flips over to the out-of-plane [100] axis while the Er moments remain unchanged, i.e., the $Dy_B[100]/Er_S[\bar{1}11]$ state. This state (B5) is the reverse of (B1).

Further evidence for the four step mechanism shown in Fig. 13 can be gleaned from the partial loops shown in Figs. 14(a) and 14(b). When the field is cycled from 10 → −2.75 → 10 T, the change in the Er-XMCD signal is large, but almost reversible. Once again we ascribe the almost reversible change in the Er signal to the existence of low energy ⟨110⟩ saddle points. However, on cycling between 10 → −5 → 10 T [Fig. 14(b)] we see large irreversible changes in both the Dy and Er-XMCD signals, as expected.

In summary, for fields applied either along the easy and hard axes, we see two very differing loops for the Er and Dy sublattices.

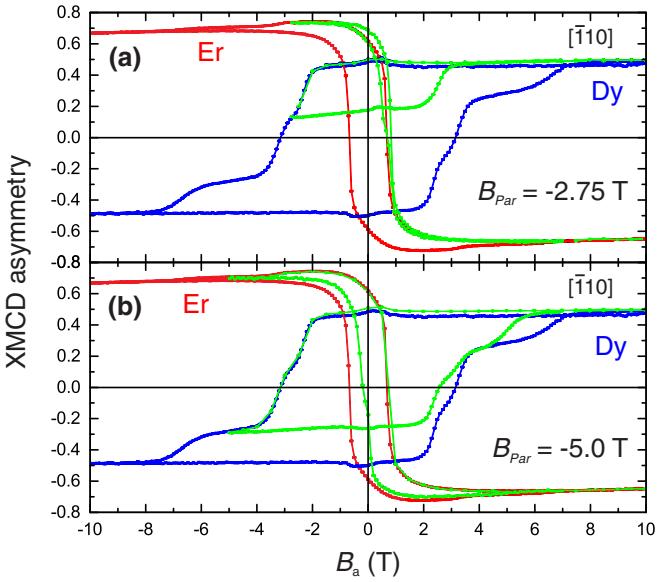

FIG. 14. (Color online) Partial loop (green) obtained by sweeping the field from (a) $10 \rightarrow -2.75 \rightarrow 10$ T and (b) from $10 \rightarrow -5 \rightarrow 10$ T, for a magnetic field applied along an in-plane [1̄10] axis.

APPENDIX D: DIAGRAMS FOR THE [1̄10] LOOP

From an examination of the energies of the (B1) → (B4) spring states shown in Fig. 15(a), it is clear that the in-plane state (B1) ($Dy_B[010]/Er_S[1\bar{1}\bar{1}]$) possesses the lowest energy in a large positive magnetic field. However, as the field is reduced to near zero, exchange spring collapse occurs and the spin-state morphs into the near AF state (B2). Once again, this state is surprisingly stable out to a negative field of some −20 T. However, it is also clear it has a higher energy than those of the out-of-plane states (B3) and (B4). Thus a transition to the (B3) and (B4) states can be anticipated as the field is taken to more negative values. What is surprising about Fig. 15(a) is the near equivalence of the energies of spin states (B3) and (B4). Rather surprisingly, this is also true for the overall magnetic moment [see Fig. 15(b)], and both the Dy and Er moments [see Figs. 15(c) and 15(d), respectively]. However, their Stoner-Wohlfarth field ranges differ slightly (see Table IV).

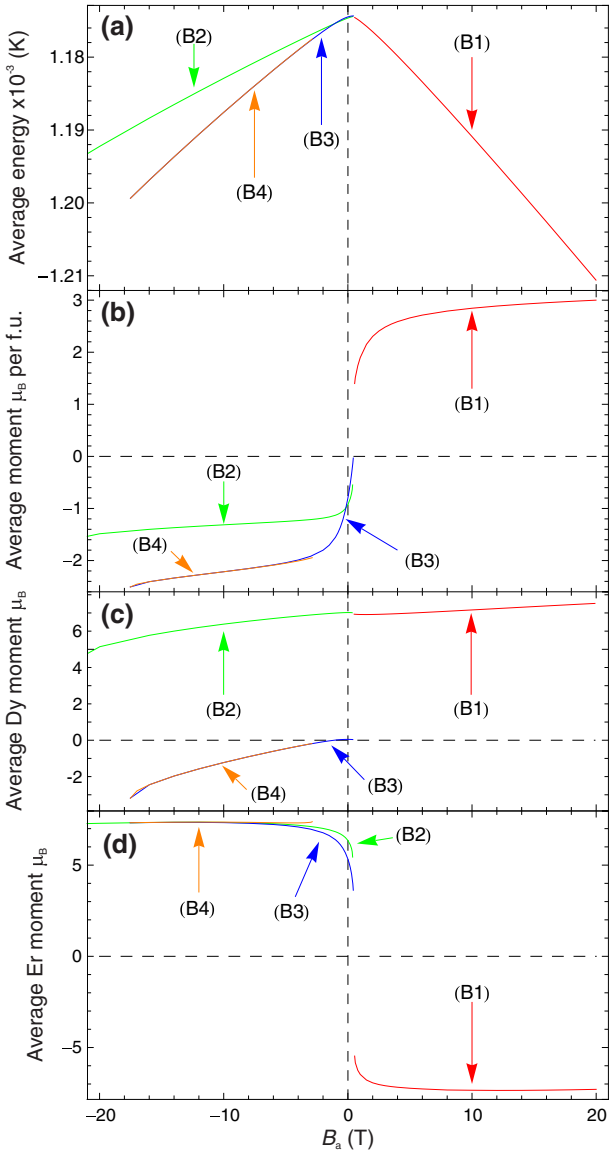

FIG. 15. (Color online) (a) Average energy per formula unit vs magnetic field, (b) average magnetic moment per formula unit vs magnetic field, (c) average Dy moment vs magnetic field, and (d) average Er moment vs magnetic field for the first four states (B1) → (B4) of Fig. 13.

[1] R. C. O'Handley, *Modern Magnetic Materials: Principles and Applications* (John Wiley & Sons, Chichester, UK, 2000).

[2] D. Craik, *Magnetism: Principles and Applications* (John Wiley & Sons, Chichester, UK, 1995).

[3] E. F. Kneller and R. Hawig, The exchange-spring magnet—A new material principle for permanent magnets, IEEE Trans. Magn. **27**, 3588 (1991).

[4] R. Skomski and J. M. D. Coey, Nucleation field and energy product of aligned 2-phase magnets—Progress towards the '1 MJ/M3' magnet, IEEE Trans. Magn. **29**, 2860 (1993).

[5] R. Skomski and J. M. D. Coey, Giant energy product in nanostructured 2-phase magnets, Phys. Rev. B **48**, 15812 (1993).

[6] R. Skomski, Aligned 2-phase magnets—Permanent magnetism of the future, J. Appl. Phys. **76**, 7059 (1994).

[7] Y. Liu, Y. Q. Wu, M. J. Kramer, Y. Choi, J. S. Jiang, Z. L. Wang, and J. P. Liu, Microstructure Analysis of a SmCo/Fe Exchange Spring Bilayer, Appl. Phys. Lett. **93**, 192502 (2008).

[8] K. Dumesnil, M. Dutheil, C. Dufour, and P. Mangin, Spring magnet behavior in $DyFe_2/YFe_2$ Laves phases superlattices, Phys. Rev. B **62**, 1136 (2000).

[9] M. Sawicki, G. J. Bowden, P. A. J. de Groot, B. D. Rainford, J.-M. L. Beaujour, R. C. C. Ward, and M. R. Wells, Exchange springs in antiferromagnetically coupled $DyFe_2$–YFe_2 superlattices, Phys. Rev. B **62**, 5817 (2000).

[10] G. van der Laan and A. I. Figueroa, X-ray magnetic circular dichroism—A versatile tool to study magnetism, Coord. Chem. Rev. **277-278**, 95 (2014).

[11] D. Wang, A. R. Buckingham, G. J. Bowden, R. C. C. Ward, and P. A. J. de Groot, Engineering irreversibility of exchange springs in antiferromagnetic $DyFe_2/YFe_2$ superlattices, Mater. Res. Express **1**, 036110 (2014).

[12] K. Dumesnil, C. Dufour, Ph. Mangin, and A. Rogalev, Magnetic springs in exchange-coupled $DyFe_2/YFe_2$ superlattices: An element-selective x-ray magnetic circular dichroism study, Phys. Rev. B **65**, 094401 (2002).

[13] K. Dumesnil, C. Dufour, Ph. Mangin, A. Rogalev, and F. Wilhelm, Temperature dependence in the magnetization reversal process of $DyFe_2/YFe_2$ exchange-coupled superlattices, J. Phys.: Condens. Matter **17**, L215 (2005).

[14] J.-M. L. Beaujour, G. J. Bowden, S. Gordeev, P. A. J. de Groot, B. D. Rainford, R. C. C. Ward, and M. R. Wells, Negative Coercivity in Epitaxially Grown (110) $DyFe_2/YFe_2$ Superlatices, Appl. Phys. Lett. **78**, 964 (2001).

[15] G. B. G. Stenning, G. J. Bowden, S. A. Gregory, P. A. J. de Groot, G. van der Laan, L. R. Shelford, P. Bencok, P. Steadman, A. N. Dobrynin, and T. Hesjedal, Transverse magnetic exchange springs in a $DyFe_2/YFe_2$ superlattice, Phys. Rev. B **86**, 174420 (2012).

[16] G. B. G. Stenning, G. J. Bowden, S. A. Gregory, J.-M. L. Beaujour, P. A. J. de Groot, G. van der Laan, L. R. Shelford, P. Bencok, P. Steadman, A. N. Dobrynin, and T. Hesjedal, Magnetic Reversal in a YFe_2-Dominated $DyFe_2/YFe_2$ Multilayer Film, Appl. Phys. Lett. **101**, 072412 (2012).

[17] D. Wang, A. R. Buckingham, G. J. Bowden, R. C. C. Ward, and P. A. J. de Groot, Meta-stable magnetic exchange spring states with negative coercivity in $DyFe_2/YFe_2$ multilayers, in *36*th *Annual Condensed Matter and Materials Conference* (Charles Sturt University, Wagga Wagga, New South Wales, Australia, 2012), p. TP16.

[18] G. B. G. Stenning, G. J. Bowden, P. A. J. de Groot, G. van der Laan, A. I. Figueroa, P. Bencok, P. Steadman, and T. Hesjedal, Magnetic reversal in Dy-doped $DyFe_2/YFe_2$ superlattice films, Phys. Rev. B **91**, 094403 (2015).

[19] S. N. Gordeev, J.-M. L. Beaujour, G. J. Bowden, B. D. Rainford, P. A. J. de Groot, R. C. C. Ward, M. R. Wells, and A. G. M. Jansen, Giant Magnetoresistance by Exchange Springs in $DyFe_2/YFe_2$ Superlattices, Phys. Rev. Lett. **87**, 186808 (2001).

[20] K. N. Martin, P. A. J. de Groot, B. D. Rainford, K. Wang, G. J. Bowden, J. P. Zimmermann, and H. J. Fangohr, Magnetic anisotropy in the cubic Laves $REFe_2$ intermediate compounds, J. Phys.: Condens. Matter **18**, 459 (2006).

[21] G. J. Bowden, P. A. J. de Groot, B. D. Rainford, K. Wang, K. N. Martin, J. P. Zimmermann, and H. J. Fangohr, Magnetic anisotropy term in [110] MBE-grown $REFe_2$ films involving the strain term epsilon(xy), J. Phys.: Condens. Matter **18**, 5861 (2006).

[22] M. J. Bentall, R. C. C. Ward, E. J. Grier, and M. R. Wells, Structure of $DyFe_2/YFe_2$ Laves phase superlattices grown by molecular beam epitaxy, J. Phys.: Condens. Matter **15**, 6493 (2003).

[23] C. Wang, A. Kohn, S. G. Wang, and R. C. C. Ward, Interlayer diffusion studies of a Laves phase exchange spring superlattice, J. Phys.: Condens. Matter **23**, 116001 (2011).

[24] B. T. Thole, G. van der Laan, J. C. Fuggle, G. A. Sawatzky, R. C. Karnatak, and J. M. Esteva, The $3d$ x-ray absorption lines and the $3d^9 4f^{n+1}$ multiplets of the lanthanides, Phys. Rev. B **32**, 5107 (1985).

[25] G. B. G. Stenning, A. R. Buckingham, G. J. Bowden, R. C. C. Ward, G. van der Laan, L. R. Shelford, F. Maccherozzi, S. S. Dhesi, and P. A. J. de Groot, Magnetization reversal processes in $ErFe_2/YFe_2$ exchange spring multilayer studied by x-ray magnetic circular dichroism, Phys. Rev. B **84**, 104428 (2011).

[26] G. J. Bowden, A. R. Buckingham, G. B. G. Stenning, and P. A. J. de Groot, Some comment on the magnetic moments used in $REFe_2$ exchange spring micro-magnetic simulations, J. Phys.: Condens. Matter **22**, 291001 (2010).

[27] M. S. S. Brooks, L. Nordstrom, and B. Johansson, $3d$-$5d$ band magnetism in rare-earth transition-metal intermetallics—Total and partial magnetic moments of the $GdFe_2$-$YbFe_2$ Laves phase compounds, J. Phys.: Condens. Matter **3**, 2357 (1991).

[28] C. Meyer, F. Hartmann-Boutron, Y. Gros, Y. Berthier, and J. L. Buevoz, Detailed study of $NdFe_2$ and additional results relative to $PrFe_2$ and YFe_2. Comparison with other R.E. compounds, J. Phys. France **42**, 605 (1981).